

Implications of emerging vehicle technologies on critical materials supply and demand in the United States

Supporting information

Tomer Fishman ¹, Rupert J. Myers ^{1,2}, Orlando Rios ³, T.E. Graedel ¹

1. Yale University, Center for Industrial Ecology, School of Forestry and Environmental Studies, 195 Prospect St. New Haven, CT 06511, USA
2. King's Buildings, School of Engineering, University of Edinburgh, Edinburgh, EH9 3JL, UK
3. Oak Ridge National Laboratory, Oak Ridge, TN, USA

Corresponding author: Tomer Fishman, tomer.fishman@yale.edu

TABLE OF CONTENTS

1	MODELING FRAMEWORK	2
2	ALLOCATION OF BATTERY TECHNOLOGIES TO DRIVE TECHNOLOGIES	2
3	MATERIAL INTENSITY COMPILATION (MASS OF MATERIALS IN A SINGLE VEHICLE)	3
3.1	Data and compilation methods	3
3.2	Method 1: compiling reported values for vehicle components	3
3.3	Method 2: averaging reported values for whole vehicles.	5
4	AEV INFLOW GROWTH CURVE	8
4.1	Selection of the top asymptote value	8
4.2	Logistic curve fitting	8
5	INFLOWS AND OUTFLOWS RESULTS OF FURTHER RARE EARTH ELEMENTS AND OTHER METALS NOT DISCUSSED IN THE ARTICLE	10
6	UNCERTAINTY AND MONTE CARLO SIMULATIONS	13
6.1	Causes of uncertainty in the model variables	13
6.2	Functional forms of the uncertainty distributions of the exogenous variables	14
6.2.1	Inflow of vehicles	14
6.2.2	Drive and battery technology share coefficients	15
6.2.3	Cohort survival curve	17
6.2.4	Material intensities	18
6.3	Uncertainty results	18
7	GLOBAL SENSITIVITY ANALYSIS AND ATTRIBUTION OF UNCERTAINTY	20
7.1	Methods	20
7.2	Sensitivity analysis results	20
7.2.1	Common findings	20
7.2.2	Neodymium	22
7.2.3	Cerium	23
7.2.4	Dysprosium	24
7.2.5	Cobalt	25
7.2.6	Lithium	26
7.2.7	Platinum	27
8	REFERENCES	28

1 Modeling framework

The modeling framework used in this research is a cohort-based dynamic flow-driven model. Figure S1 presents a conceptual diagram of the model. In line with the Material Flows Analysis (MFA) perspective, stocks and flows can be tracked as either goods (in this case, vehicles) and materials/substances (in this case, critical materials) [1]. The material intensity (MI) coefficients – mass of material per a single unit of a good – enable conversion between goods and substances. In this sense, inflows refer to both new vehicle sales and their material demands. The vehicle fleet forms the in-use reservoir of these materials (“urban mine”), and the outflows of end-of-life vehicles are a stream of potential recyclable materials that can serve as a secondary supply source to augment primary supply from mining production.

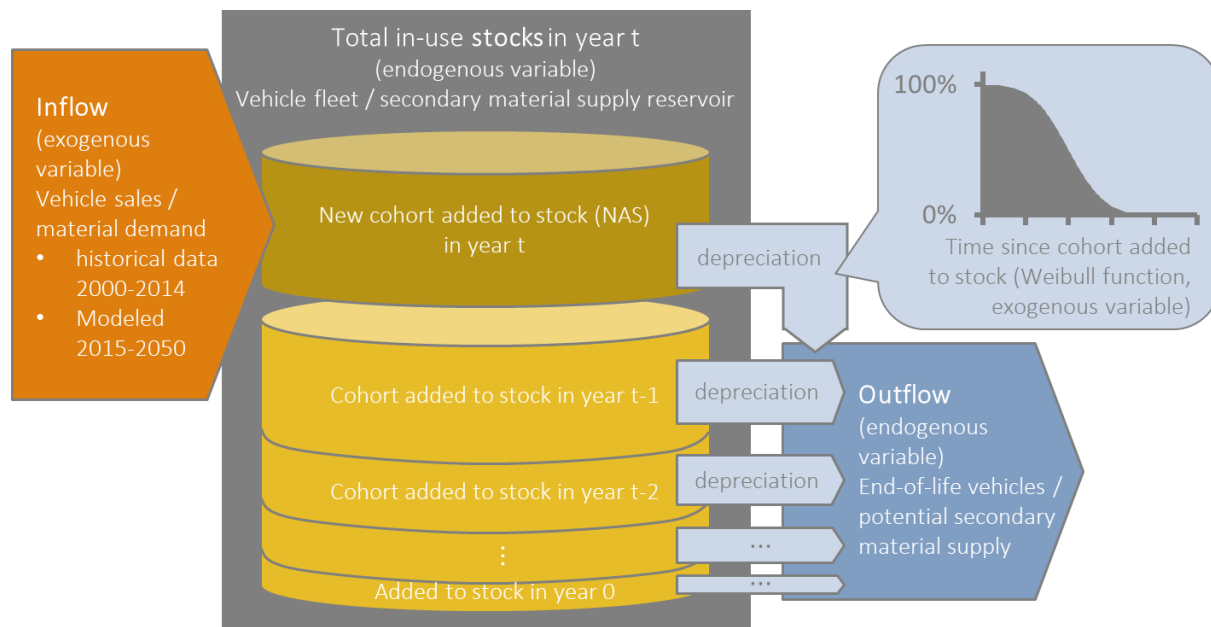


FIGURE S1: A CONCEPTUAL DIAGRAM OF THE MODEL FRAMEWORK. ADAPTED FROM FISHMAN ET AL. [2]

2 Allocation of battery technologies to drive technologies

The BLUE map does not describe the types of batteries used with each drive technology. We therefore dynamically assigned battery technologies to the four drive technologies as follows: PHEV and BEV vehicles have so far used lithium ion (Li-ion) batteries so we assume they will continue to do so. Most current HEV vehicles use NiMH batteries, but the shares of Li-ion and Li-polymer (Li-poly) batteries have been increasing. We extrapolate these apparent trends so that by 2050 the share of HEV batteries in new vehicles will be NiMH=10%, Li-ion=50%, and Li-poly=40%. For FCVs there are no historical battery data available, so we assume equal shares of Li-ion, Li-poly, and NiMH batteries.

3 Material intensity compilation (mass of materials in a single vehicle)

3.1 Data and compilation methods

Material intensity data for vehicles were compiled to represent the range of commercial light duty vehicles in the United States. These vehicles are internal combustion engine vehicles (ICEVs), hybrid electric vehicles (HEVs), plug-in hybrid electric vehicles (PHEVs), battery electric vehicles (BEVs), and fuel cell vehicles (FCVs) [3], each with allocated battery technologies as described above. These data were compiled independently in two ways.

3.2 Method 1: compiling reported values for vehicle components

In this method, MIs of various vehicle components were compiled from reported values for vehicle components to match standard model vehicle configurations for each type, ICEV, HEV, PHEV, BEV, and FCV. The material intensities of their components were then summed to create the MI of the entire vehicle.

Calculations of vehicle material intensities employed the ICEV, HEV (parallel configuration with one electric motor and generator), PHEV (series configuration with two electric motors and generators), BEV (one electric motor and generator), and FCV configurations reported by Chan et al. [4]; the FCV and BEV configurations are similar but the former additionally contains a fuel cell. Vehicle models were selected from the U.S. Department of Energy's Alternative Fuels Data Center (AFDC) [3]; model specifications were taken from the AFDC if available, or from manufacturer brochures otherwise [5–10]; battery data such as type, number of cells, and voltage were obtained from the U.S. Department of Energy [11]. Data for vehicle models manufactured between 2006 and 2017 were used, with an average model year of 2013.

The elemental composition of a Li-ion battery [12] was used to describe both Li-ion and Li-polymer battery models; this battery contains a $\text{Li}(\text{Ni}_{1/3}\text{Co}_{1/3}\text{Mn}_{1/3})\text{O}_2$ cathode, a graphite anode, two parallel sub-packs, a total weight of 253 kg of which 151.8 kg (60 mass%) is comprised of 360 cells in 12 modules, a capacity of 26.6 kWh, and a 95-96% efficiency. Elemental compositions for the NiMH battery were determined using a model NiMH battery with 190 cells of 1.2 V each, 55 Wh/kg, and a total mass of 32.7 kg [13]. The mass of each model NiMH battery cell was assigned by dividing the 43.4 kg NiMH battery described in Yano et al. [14] by the number of cells (252), which was then scaled using the average number of NiMH battery cells in the sampled commercial vehicles (190 cells) to obtain the total NiMH battery mass of 32.7 kg. The average elemental compositions of each battery type in each manufactured vehicle model, i.e., Li-ion, Li-polymer, and NiMH in HEVs, PHEVs, BEVs, and FCVs, were determined by linearly scaling these battery data to match the manufacturer reported battery sizes.

The other vehicle components used in calculations are a synchronous electric motor and a generator, a fuel cell, an ICEV engine and related parts, and the vehicle body excluding the powertrain (body and doors, brakes, chassis, final assembly, interior and exterior, and tires and wheels, which together are referred to as the glider in Hawkins et al. [15]). We chose to use synchronous (rather than induction)

electric motors and generators because data for them are readily available [14,15] and because they presently occur in most alternative energy vehicles in the United States. We acknowledge that this preference for synchronous motors may change in the future, and also that these data represent upper estimates of permanent magnet use in electric motors and generators (due to the absence of including induction motors here). Dy, Nd, and Pr compositions in the model electric motor and generator were determined by averaging their reported contents in Yano et al. [14] due to the absence of Dy and Pr data in Hawkins et al. [15,16]. Data from Hawkins et al. [15,16] were otherwise taken. Elemental compositions for the ICEV engine and glider were obtained from Hawkins et al. [15,16]. The value of 2 g of platinum in catalytic converters (in ICEVs, HEVs, and PHEVs) was chosen based on ranges of 1-4 g [17–19], acknowledging the fact that it can be substituted for palladium depending on market prices. Fuel cells were specified to contain 20 g Pt [20,21]. A steel composition of 98.5 mass% Fe, 1.3 mass% Mn, and 0.2 mass% C was used in all vehicle models.

MIs in the scale of kilograms and above were rounded to hundreds of grams. MIs in smaller scales were rounded to two significant digits. The masses of 20 elements in each component are summed in table S1.

TABLE S1: MASSES OF MATERIALS IN COMPONENTS OF INTERNAL COMBUSTION AND ALTERNATIVE ENERGY VEHICLES. UNIT: GRAMS.

	Electric motor + generator	Fuel cell	Internal combustion engine + powertrain	"Glider" (body and doors, brakes, chassis, final assembly, interior and exterior, and tires and wheels)	Li-ion battery (HEV, FCV)	Li-ion battery (PHEV)	Li-ion battery (BEV)	Li-poly battery (HEV, FCV)	NiMH battery (HEV, FCV)
Li	-	-	-	-	206	2571	7466	354	17
Mg	-	-	-	200	-	-	-	-	-
Al	43210	-	49500	21800	376	4686	13607	645	-
Cr	-	-	-	-	-	-	-	-	559
Mn	2095	-	1130	10022	526	6562	19054	902	-
Fe	131968	-	144406	777537	-	-	-	-	2300
Co	-	-	-	-	564	7039	20439	968	-
Ni	-	-	-	-	562	7011	20356	964	9492
Cu	14000	-	6500	15800	1731	21604	62729	2971	-
Zn	-	-	-	100	-	-	-	-	-
La	-	-	-	-	-	-	-	-	536
Ce	-	-	-	-	-	-	-	-	740
Pr	0.5	-	-	-	-	-	-	-	74
Nd	497	-	-	-	-	-	-	-	234
Gd	-	-	-	-	-	-	-	-	5
Tb	-	-	-	-	-	-	-	-	0.24
Dy	34	-	-	-	-	-	-	-	0.12
Er	-	-	-	-	-	-	-	-	0.25
Pt	-	20	2	-	-	-	-	-	-
Pb	10	-	-	300	-	-	-	-	-

The total masses of the model ICEV, HEV, PHEV, and AEV that were obtained by summing their component masses are ~200-400 kg below the specified curb weights of similar vehicles (table S3). This range is consistent with the 266 and 282 kg total mass of glass, plastic, rubber, paint and other non-metallic materials in the BEV and ICEV, respectively, investigated in Hawkins et al. [15,16]. The model

FCV is ~800 kg below the specified curb weight of the 2017 Toyota Mirai [9] (a commercially available FCV); this missing mass is related both to non-metallic materials and also to the fuel cell, for which only Pt was included here due to lack of data for other elements.

As mentioned in the main text, smaller components with high variability between vehicle models, such as motors for automatic windows or navigation and audio systems are not included even though they may include small amounts of materials which could be of interest [22,23] because of their high variability and challenge of plausible assumptions about their future trends.

Method 1 includes 20 elements and more reliably accounts for differences in battery size and type, and vehicle configuration, both of which vary substantially depending on the model vehicle, and is the dataset used in this study. Table S2 presents the MI values obtained with method 1 for ICEV and the eight AEV technologies.

TABLE S2: MATERIAL INTENSITY VALUES FOR THE MASS OF MATERIALS IN THE VARIOUS VEHICLE DRIVE TECHNOLOGY AND BATTERY COMBINATIONS OBTAINED USING METHOD 1. THE RARE EARTH ARE MARKED IN BOLD, AND THE FOUR MATERIALS WHOSE INTENSITIES ARE MODIFIED IN THE Fe SUBSTITUTION SCENARIO SET AND Al SUBSTITUTION SCENARIO SET ARE IN ITALICS. NOTE THAT CERIUM IS BOTH BOLD AND ITALIC. UNIT: GRAMS.

	ICEV	HEV NiMH	HEV Li-ion	HEV Li-polymer	PHEV Li-ion	BEV Li-ion	FCV NiMH	FCV Li-ion	FCV Li-polymer
Li	-	17	210	350	2600	7500	17	210	350
Mg	200	200	200	200	200	200	200	200	200
<i>Al</i>	<i>71300</i>	<i>114500</i>	<i>114900</i>	<i>115200</i>	<i>162400</i>	<i>78600</i>	<i>65000</i>	<i>65400</i>	<i>65700</i>
Cr	-	560	-	-	-	-	560	-	-
Mn	11200	13200	13800	14100	21900	31200	12100	12600	13000
<i>Fe</i>	<i>921900</i>	<i>1056200</i>	<i>1053900</i>	<i>1053900</i>	<i>1185900</i>	<i>909500</i>	<i>911800</i>	<i>909500</i>	<i>909500</i>
Co	-	-	560	970	7000	20400	-	560	970
Ni	-	9500	560	970	7000	20400	9500	560	960
Cu	22300	36300	38000	39300	71900	92500	29800	31500	32800
Zn	100	100	100	100	100	100	100	100	100
<i>La</i>	-	<i>540</i>	-	-	-	-	<i>540</i>	-	-
<i>Ce</i>	-	<i>740</i>	-	-	-	-	<i>740</i>	-	-
<i>Pr</i>	-	<i>74</i>	<i>0.5</i>	<i>0.5</i>	<i>1</i>	<i>0.5</i>	<i>74</i>	<i>0.5</i>	<i>0.5</i>
<i>Nd</i>	-	<i>730</i>	<i>500</i>	<i>500</i>	<i>1000</i>	<i>500</i>	<i>730</i>	<i>500</i>	<i>500</i>
<i>Gd</i>	-	<i>5</i>	-	-	-	-	<i>5</i>	-	-
<i>Tb</i>	-	<i>0.24</i>	-	-	-	-	<i>0.24</i>	-	-
<i>Dy</i>	-	<i>34.1</i>	<i>34</i>	<i>34</i>	<i>68</i>	<i>34</i>	<i>34.1</i>	<i>34</i>	<i>34</i>
<i>Er</i>	-	<i>0.25</i>	-	-	-	-	<i>0.25</i>	-	-
Pt	2	2	2	2	2	-	20	20	20
Pb	300	310	310	310	320	310	310	310	310
Sum	1027302	1233013	1223077	1225937	1460391	1161245	1031531	1021495	1024445

3.3 Method 2: averaging reported values for whole vehicles.

In this method MIs were obtained by averaging reported values for whole vehicles [15,16,22,24–27]. MIs in the scale of kilograms and above were rounded to hundreds of grams. MIs in smaller scales were rounded to two significant digits. Method 2 resulted in MIs for 41 elements of which 7 are only reported

for ICEVs which are not part of this study. This method also did not provide data for the FCV drive technology and Li-polymer battery technology. Moreover, it does not differentiate vehicle components, required for the *Fe substitution scenario*, and so was only used for benchmarking and confirmation of the numbers obtained with method 1, and is included here for reference. Table S3 presents the values obtained with method 2, and Table S4 compares the two methods with the specified curb weight of vehicle models, as reported by their makers.

TABLE S3: MI VALUES OBTAINED WITH METHOD 2, BY AVERAGING REPORTED VALUES FOR WHOLE VEHICLES. UNIT: GRAMS. ELEMENTS WITH AN ASTERISK (*) DO NOT APPEAR IN THE MI TABLE OBTAINED WITH METHOD 2 (TABLE S2).

	ICEV	HEV NiMH	HEV Li-ion	PHEV Li-ion	BEV Li-ion
Li	5.5	-	-	6300	5700
Mg	5300	-	-	9100	200
Al	102000	75000	80000	160000	217000
Ar *	0.01	-	-	-	-
Sc *	1.1	-	1.05	-	-
V *	59	-	-	-	-
Cr	6500	-	-	-	-
Mn	8700	14600	14400	14600	25200
Fe	1036300	1217300	1207400	1266500	803700
Co	64	-	-	70	15700
Ni	1800	-	-	-	15600
Cu	26700	105000	100000	88500	173900
Zn	100	-	-	-	100
Ga *	0.29	-	-	0.57	-
Sr *	190	-	-	-	-
Y *	0.26	-	0.60	0.23	-
Zr *	8	-	-	-	-
Nb *	93	-	-	110	-
Mo *	470	-	-	630	-
Rh *	0.01	0.01	-	0.01	-
Pd *	3.5	1.8	-	1.8	-
Ag *	19	-	-	50	-
In *	0.15	-	-	0.08	-
Sb *	46	-	-	-	-
La	2.8	738	8.1	6.7	-
Ce	27	1100	82	36	-
Pr	9.9	-	30	4	-
Nd	120	980	520	490	790
Sm *	1	-	3.3	1.4	-
Eu *	0.12	-	0.46	0.01	-
Gd	0.10	-	0.35	0.01	-
Tb	0.007	-	0.001	20	-
Dy	12	260	160	190	370
Er	0.18	-	-	0.18	-
Yb *	0.11	-	0.0017	0.16	-
Ta *	6.4	-	-	11	-
W *	0.17	-	-	-	-
Pt	5.4	5.5	-	5.5	-
Au *	6	-	-	5.8	-
Hg *	0.01	-	-	-	-
Pb	280	-	-	-	300
Sum	1188831	1414985	1402606	1546633	1258560

TABLE S3: COMPARISONS OF THE TOTAL MASS OF VEHICLES OBTAINED WITH METHODS 1 & 2 (ROUNDED TO KG), AND REPORTED SPECIFIED CURB WEIGHTS OF VEHICLES.

	ICEV	HEV NiMH	HEV Li-ion	HEV Li-polymer	PHEV Li-ion	BEV Li-ion	FCV NiMH	FCV Li-ion	FCV Li-polymer
Method 1	1030	1230	1220	1230	1460	1160	1030	1020	1020
Method 2	1188	1415	1402	n.a.	1546	1259	n.a.	n.a.	n.a.
Specified curb weight (model)	1470 (Toyota Camry) [5]	1380 (Toyota Prius) [6]	1380 (Toyota Prius) [6]	1380 (Toyota Prius) [6]	1718 (Kia Optima PHEV) [7]	1500 (Nissan Leaf) [8]	1848 (Toyota Mirai) [9]	1848 (Toyota Mirai) [9]	1848 (Toyota Mirai) [9]

4 AEV Inflow growth curve

4.1 Selection of the top asymptote value

The objective of the statistical analysis in this section is to rule out patterns of growth or decline in this time series, to corroborate the use of the average as the top asymptote of the AEV sales growth curve. Inflow time series of total light duty vehicles (ICEVs and non-ICEVs) in the USA 1992-2014 was obtained from the U.S. Department of Transportation [28]. The average in this period is 7.76 million per year.

We analyzed the time series to determine whether it is stationary, i.e. “one whose properties do not depend on the time at which the series is observed.” [29]. We conducted this analysis using standard time-series analysis procedures [29] with R’s forecast package. The Autocorrelation Function (ACF) plot of the total light duty vehicle sales time series indicated non-stationarity, supported by both the Adjusted Dickey-fuller (ADF) test and Kwiatkowski-Phillips-Schmidt-Shin (KPSS) tests which indicated a unit root in the time series.

The differenced series ($inflow(t) - inflow(t - 1)$) was found to have no unit root using the same tests. Analysis of the differenced series indicated that it is stationary with a mean of zero, i.e. this series has no constant, and thus the original time series exhibits no deterministic “drift” –no systematic growth or decline trends. Although this means that random shocks may have permanent effects on the level of the series, we found no impediment to using the simple average of 7.76 as the total yearly inflow towards which AEV inflows approach.

Note: the ARIMA model selection procedure [29] suggests that the time series is not a random walk but rather follows an ARIMA(0,1,3) pattern which results in a constant point forecast of 7.53 million. However, obtaining a more accurate forecast of the series is beyond the aims and needs of this study, and in any case does not change the finding that there is no growth or decline trend in the time series.

4.2 Logistic curve fitting

A logistic curve was fitted using Stata 14’s NL command [30]. The general logistic curve formula is

$$y(t) = \frac{a}{(1 + e^{-B(t-M)})^{1/v}}$$

where, as described above and in the Methods and Data section of the main text, a is the top asymptote set to a value of 7.76 million, M is the point in time with the highest growth (inflection), B affects the rapidness of growth (the slope), t is the year, $y(t)$ is $inflow(t)$, and v affects the symmetry of the curve.

v was set to 1, symmetrical growth rate. The historical data series was found to be too short (and small in comparison to the top asymptote) to provide information that would help choose a value for v : the AIC and BIC statistics, were nearly identical even with extremely asymmetrical values of v (i.e. 0.5, 2) (Figure S2), suggesting that any value of v , at least within this range, is plausible. A value of $v = 1$ was chosen for considerations of parsimony.

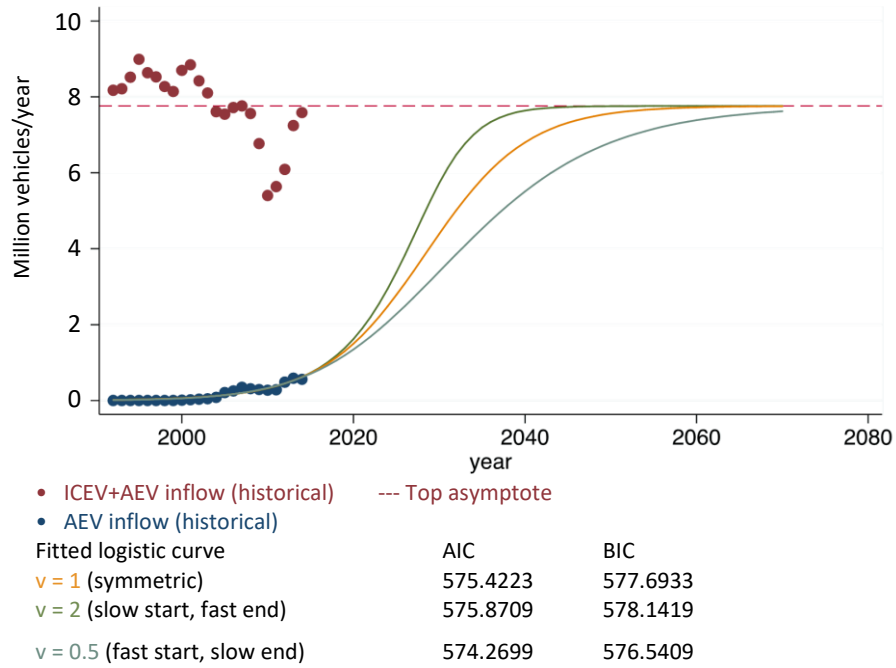


FIGURE S2: COMPARISON OF THREE LOGISTIC CURVES FITTED TO THE HISTORICAL AEV INFLOW DATA AND 7.76×10^6 TOP ASYMPTOTE, WITH DIFFERENT VALUES OF v . ALSO SHOWN ARE THE AIC AND BIC STATISTICS OF THE THREE FITTED CURVES.

5 Inflows and outflows results of further rare earth elements and other metals not discussed in the article

Figures S3-S4 present the inflow and outflow curves obtained for Tb, Er, Gd, Pr, and Dy; and Pt, Cr, Zn, Mg, Pb, Li, Co, Ni, Mn, Cu, Al, and Fe, respectively, in the baseline scenario.

Several observations can be made from these figures, as noted for each element below.

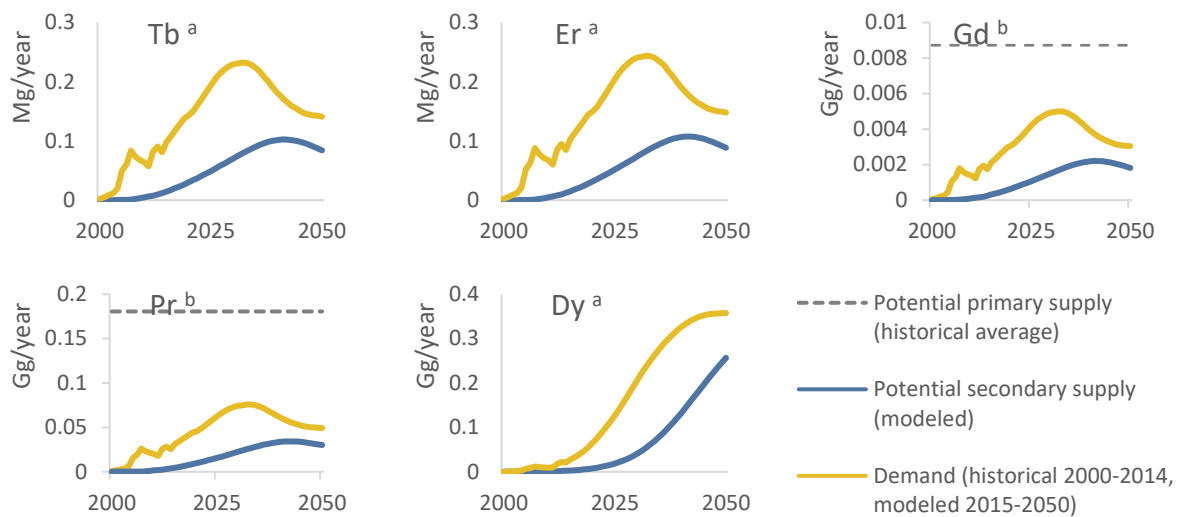


FIGURE S3: THE DEMANDS BY AEV INFLOWS AND POTENTIAL SECONDARY SUPPLIES FROM END-OF-LIFE AEV OUTFLOWS OF THE RARE EARTH ELEMENTS Tb, Er, Gd, Pr, AND Dy IN THE USA, 2000-2050, AND HISTORICAL (2012-2015) AVERAGE DOMESTIC PRIMARY PRODUCTION (Gd AND Pr ONLY) SUPERIMPOSED. NOTE THE DIFFERENT ORDINAL SCALES.

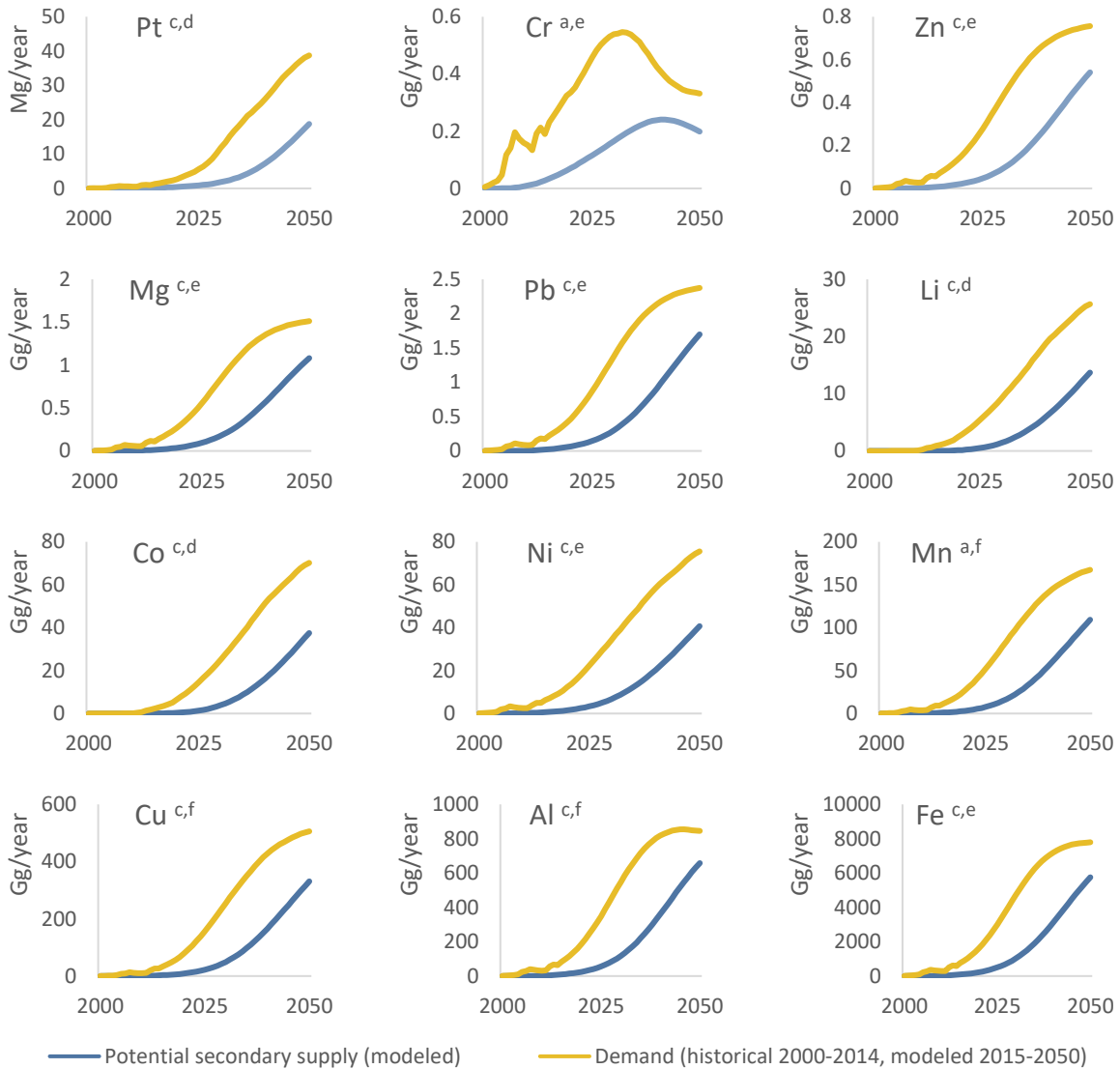


FIGURE S4: THE DEMANDS BY AEV INFLOWS AND POTENTIAL SECONDARY SUPPLIES FROM END-OF-LIFE AEV OUTFLOWS OF PT, CR, ZN, MG, PB, NI, MN, CU, AL, IN THE USA, 2000-2050. NOTE THE DIFFERENT ORDINAL SCALES.

Observations from Figures S3-S4 (referencing information from the USGS 2017 Mineral Commodities Summaries [31]):

- a. Terbium, Erbium, Dysprosium, Chromium, and Manganese have no primary production in the USA.
- b. Gadolinium and Praseodymium currently have no primary production in the USA, but were mined from 2012-2015 at the Mountain Pass mine with other rare earth metals. See the main text for discussion.
- c. Platinum, Zinc, Magnesium, Lead, Lithium, Cobalt, Nickel, Copper, Aluminum, and Iron have primary production in the USA. Magnesium’s primary production figures are withheld.
- d. Platinum, Lithium, and Cobalt demands by AEVs and eventual end-of-life availability from AEVs in our scenarios exceed historical US average production levels by orders of magnitude, resembling neodymium trends discussed in the main text.

- e. Chromium, Zinc, Magnesium, Lead, Nickel, and Iron's current (2012-2017) overall apparent consumption levels (consisting of imports, recycling, and primary production) are orders of magnitude higher than the demands and supply of the AEV sector in our scenarios.
- f. Manganese, Copper, and Aluminum in our scenarios reach maximum demands that would equal about 20% (Mn), 28% (Cu), and 17% (Al) of current consumption levels. It should be noted that currently 19% of copper consumption and 41% of aluminum consumption in the USA are already by transportation applications (which include light duty vehicles).

It would seem that, beside the materials discussed in the main text, Pt, Li, Co, and Mn could be of some concern and warrant further study.

6 Uncertainty and Monte Carlo simulations

This model is deterministic: the initial values of the exogenous variables fully determine the results through the set of equations. Any uncertainties inherent in these variables would propagate through the model to the endogenous variables (the results). The explorative nature of the model, which focuses on potential futures, lends itself to an approach of Monte Carlo simulations. This approach has been commonly used in dynamic flow-stock models [32–34]. In this method the value of each exogenous variable is stochastically drawn from a probability distribution in which the original point estimate is the median value. This action creates a new model-run with somewhat different starting points and therefore new results. This process is repeated numerous times. The resulting endogenous variables of all runs are statistically analyzed to derive uncertainty ranges in the results, identify the sensitivity of results to variance and uncertainty in each exogenous variable, track these changes through the model time steps, and compare variables' relative influence on results. For further description of the method, the reader is referred to textbooks on the subject of uncertainty [35]. We executed a series of Monte Carlo simulations with 10^3 runs, which were found to be sufficient for values to converge and produce uncertainty bands to be analyzed. The following sections detail the steps taken.

6.1 Causes of uncertainty in the model variables

Laner et al. [33] suggested seven types of sources of uncertainty in material flow analysis: (1) statistical variation, (2) variability, (3) inherent randomness and unpredictability, (4) subjective judgment, (5) disagreement, (6) linguistic imprecision, and (7) approximation. We use these definitions to characterize the sources of uncertainty in our variables.

The objective of this study is the future, and as such all variables have an inherent level of uncertainty directly related to the fact that the future has yet to happen. However, the exogenous variables can be split into two groups. The first group are scenario variables, which are set to specific “what-if” values as part of the storylines we wish to analyze in this study. These include $v_{i,t}$ and $inflow(t)$ for the future ($2015 \leq t \leq 2050$) as well as the parameters used to create the $inflow(t)$ time series (the top asymptote and logistic curve parameters). These variables are based on the premises of our scenarios and not on forecasts, in part because forecasts of AEV adoption in the USA seem to be inconclusive [36] and lack systematic uncertainty analyses. The main cause of uncertainty for these variables is inherent randomness and unpredictability – they are fundamentally uncertain because they haven't happened yet. The main question is rather whether the assumptions and scenario premises we chose to use are likely storylines, which relate to the causes that Laner et al. [33] refer to as subjective judgement involved in the scenario set-up and approximation involved in the simplification of the variables.

On the other hand, the second group of exogenous variables are estimates of current and past trends. These include $MI_{i,j}$ in scenario 1 and the Weibull survival curve parameters. These variables were assembled from multiple sources as described in the main text and sections 1 and 2 of the supporting information document. Some uncertainty assessments for certain materials exists. For example, Du et al. [27] discussed the discrepancy of MIs of several critical materials as reported in different publications, but did not provide distribution statistics that could inform an empirical uncertainty analysis. The

heterogeneous methods employed in the original sources, and the varying level of uncertainty analyses – if any – supplied with the original data make reconciliation of the causes of uncertainty very difficult. We are not aware of a single integrated assessment that covers all the variables as they are used in our study. As a group, it would seem safe to conclude that all seven types of uncertainty may be evident to some extent in each of these variables. Our processing of these data, such as the synthesis of the MI coefficients, are characterized mainly by a process of approximation, in which the simplification of a single coefficient per vehicle technology removed any variance that existed between different models.

6.2 Functional forms of the uncertainty distributions of the exogenous variables

In the case of both groups of variables, the existing information on reliability was insufficient to describe empirically the range of uncertainty, let alone answer whether this uncertainty can be described by any probability distribution. The lack of readily-available uncertainty distributions in the literature led us to choose normal distributions to describe the potential variance and uncertainty in the values of the variables. Normal distributions have several favorable characteristics that make them preferable over other distributions in this case:

1. Their form is a function of only two variables (the mean and standard deviation, SD) and because we set the point estimates to be the mean there is only one parameter (SD) left to define.
2. They are symmetrical (the probability of a negative deviation from the mean is equal to the probability of positive deviation).
3. They are relatively simple to compute and interpret.
4. The multiplication of a normal distribution by a constant results in another normal distribution, an attribute we use in several instances.
5. This assumption of normal distribution for the uncertainty of the variables conforms to the central limit theorem.

Uncertainty was introduced to a total of 12 exogenous variables as described below. Each of the variables has its own normal distribution function independent of the others. However, there are some commonalities between them. The functional forms of all the normal distributions is $X \sim \mathcal{N}(\mu, (0.1\mu)^2)$, i.e. X is randomly drawn from a normal distribution with a mean μ and standard distribution (σ) which is a tenth of the mean. Time-variant variable series (e.g. $inflow(t)$ and $v_{i,t}$) were multiplied by an X drawn once per model run, which scales the entire time series. This was done rather than having a new random X drawn for each time step t because the latter option would only introduce “noise” to the time series. The overall time series would still closely resemble the original point estimates resulting in very narrow confidence intervals that do not describe the uncertainty of the time series appropriately.

We proceed to detail the uncertainty distributions modeled for each exogenous variable.

6.2.1 Inflow of vehicles

Future $inflow(t)$ data ($2015 \leq t \leq 2050$) is based on a logistic curve as explained in the methods section of the main text and section 2 of the supporting information. The fitting algorithm used to create

the curve provides statistics (e.g. standard errors and confidence intervals) which can be used to describe the uncertainty of the value of $inflow(t)$ for any t . However, the fitting algorithm accepts the top asymptote (maximum yearly vehicle inputs) as a fixed number and thus the fitting results' confidence intervals converge and become smaller starting from the inflection point as the curve gets closer to this value (i.e. as t increases), as seen in figure S5. We reason that the uncertainty should increase over time rather than decrease, and that there is a certain level of uncertainty inherent in the choice of the top asymptote which is not captured by the fitting algorithm. This was achieved by scaling the point estimate series $inflow(t)$ by a value obtained from a normal distribution once per model run:

$$inflow(t)_{MC} = inflow(t) \times S$$

$$S \sim \mathcal{N}(1, 0.1^2)$$

Where $inflow(t)_{MC}$ is the value of the inflow time series in run number MC of the Monte-Carlo simulation and S is a random value drawn from a normal distribution with a mean of 1 and variance of 0.01 (SD=0.1). The 95% confidence bands obtained with these parameters are slightly narrower those of the fitting algorithm in the growth period but continue to increase with time rather than decrease when the series stabilizes.

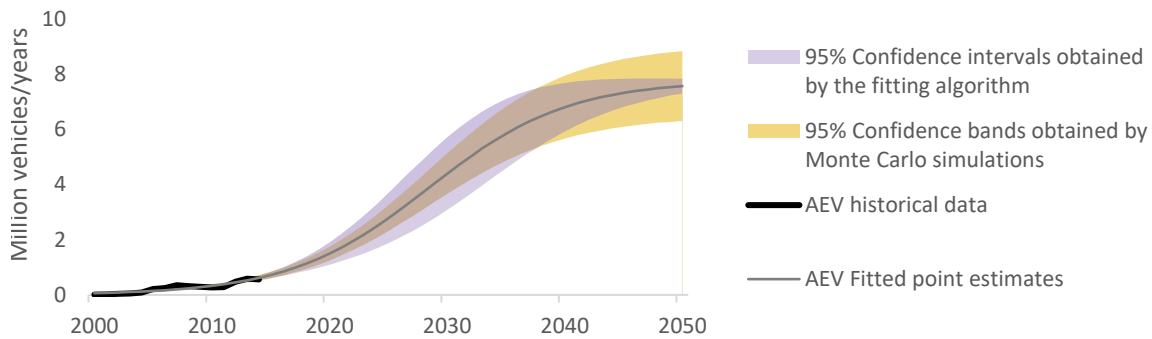


FIGURE S5: THE TOTAL AEV INFLOW (CF. FIGURE 1 IN THE ARTICLE) AND CONFIDENCE BANDS OBTAINED BY THE CURVE FITTING ALGORITHM OVERLAID BY THOSE OBTAINED BY THE MONTE CARLO SIMULATIONS, WHICH ARE THE ONES WE USE IN OUR UNCERTAINTY ANALYSIS.

6.2.2 Drive and battery technology share coefficients

The variable set $v_{i,t}$ includes the share of 8 drive and battery technology combinations. As described in the article, these shares were calculated in two steps. First, the shares of the four drive technologies (HEV, PHEV, BEV, and FCV) were derived from the IEA BLUE map. Then the battery shares of HEV and FCV were appraised based on the assumptions described in the methods section.

$$v_{i,t} = d_{k,t} \times b_{k,l,t}$$

Where d is the share of drive technology $k = \{HEV, PHEV, BEV, FCV\}$, originally derived from the IEA BLUE map, and b is the share of battery technology within each drive technology category $l = \{NiMH, Li - ion, Li - poly\}$.

We deemed that the drive technologies and battery technologies have underlying uncertainties which are independent of each other and introduce stochasticity in both calculation steps.

6.2.2.1 Drive technology shares

Randomness related to the uncertainty in the share of technologies was introduced in the following manner:

$$d_{k,t,MC} = \frac{d_{k,t} \times X_k}{\sum_k (d_{k,t} \times X_k)}$$

$$X_k \sim \mathcal{N}(1, 0.1^2)$$

Where $d_{k,t,MC}$ is the value of the inflow time series in run number mc of the Monte-Carlo simulation, rescaled to ensure that $\sum_k d_{k,t,MC} = 1$. For PHEV and BEV, b_{PHEV} and $b_{BEV,Li-ion,t} = 1$ and so no further calculation is done for these two battery technologies.

6.2.2.2 FCV Battery technology shares

For FCV, uncertainty to the assumption of equal shares (1/3, invariant over time) of the three battery types is introduced in the following manner:

$b_{FCV,l,MC} \sim \mathcal{N}\left(\frac{1}{3}, \frac{1}{30^2}\right)$ for l battery types NiMH and Li-ion (each drawn independently of the other) and for all t time steps.

And $b_{FCV,Li-poly,MC} = 1 - (b_{FCV,NiMH,MC} + b_{FCV,Li-ion,MC})$ to ensure that battery shares sum to 1. Note that $b_{FCV,Li-poly,MC}$ is also normally distributed due to the summing properties of normal distributions.

6.2.2.3 HEV Battery technology shares

HEV battery shares vary over time, and were originally set to a ratio of 5:4:1 in 2050 for Li-ion, Li-poly, and NiMH respectively. Uncertainty was introduced in the following manner:

$$b_{HEV,Li-ion,2050,MC} \sim \mathcal{N}\left(\frac{1}{2}, \frac{1}{20^2}\right)$$

$$b_{HEV,NiMH,2050,MC} \sim \mathcal{N}\left(\frac{1}{10}, \frac{1}{100^2}\right)$$

$$b_{HEV,Li-poly,2050,MC} = 1 - (b_{HEV,NiMH,2050,MC} + b_{HEV,Li-ion,2050,MC})$$

The latter to ensure that battery shares sum to 1. Note that $b_{HEV,Li-poly,MC}$ is also normally distributed due to the summing properties of normal distributions .

In each Monte Carlo run, the time series was filled from the historical 2014 data to 2050 using linear extrapolation, same as described in the methods section of the main text.

6.2.3 Cohort survival curve

The survival curves of all vehicle types and all cohorts is a Weibull distribution. Uncertainties related to survival curves in dynamic inflow-driven stock-flow models were discussed in detail in several publications [34,37,38].

The Weibull function we use is a synthesis of Weibull functions obtained from Yano et al. [14] for hybrid vehicles in Japan and Weibull functions fitted by us to the general light-duty vehicles survivability of the American passenger car fleet [39], which is mostly composed of ICEVs. Yano et al. provide Weibull functions fitted for each production year of the Toyota Prius in Japan, and we truncated newer years (which suggest longer-lasting vehicles with median lifespans of 18 years or more) because we believe there are not enough data points yet to produce good fits. Unfortunately, Yano et al. did not provide any supplementary statistics to inform about the uncertainties in their calculations. Because of good fit, the uncertainty statistics accompanying the fitted Weibull function were deemed to be too conservative to account for the uncertainties that should be expected of the lifetime distribution of an emerging technology like AEVs. To account for the high expected uncertainties, we introduced a stochastic factor to the two parameters (the shape parameter a_1 and scale parameter a_2) of the Weibull function. The uncertainties of the parameters were drawn from normal distributions:

$$a_{1,MC} \sim \mathcal{N}(2.43, 0.243^2)$$

$$a_{2,MC} \sim \mathcal{N}(16.94, 0.1694^2)$$

Each of the parameters influences the curve of the Weibull function in a non-linear fashion, and are also quite sensitive to changes in each other. Randomizing both parameters results in an extensive variety of survival curves with different acceleration and deceleration patterns and different medians. For example, the point estimate's median is 14.5 years, and the medians of the 95% intervals range from 12 to over 17 years. Because two parameters are randomized, the results are a two-dimensional uncertainty gradient which we visualize as two confidence bands in figure S6.

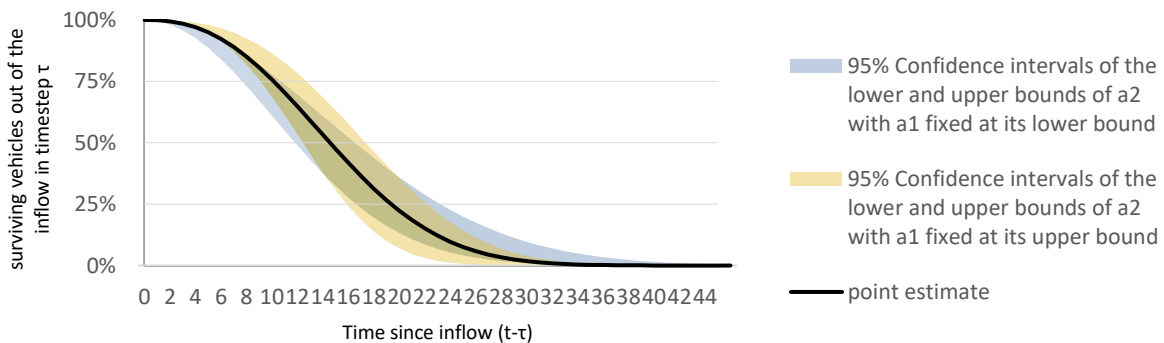


FIGURE S6: 95% CONFIDENCE BANDS FOR THE SURVIVAL CURVE OBTAINED USING MONTE CARLO SIMULATIONS. TWO CONFIDENCE BANDS ARE SHOWN TO REPRESENT THE POSSIBLE COMBINATIONS OF THE TWO RANDOMIZED PARAMETERS. IN OTHER WORDS, THE FOUR UNCERTAINTY BOUNDS PRESENTED HERE (TWO FOR EACH BAND) HAVE EQUAL PROBABILITY.

6.2.4 Material intensities

As explained in the methods section of the main text and section 1 of the supporting information, the material intensity (MI) coefficients are based on the components of a typical vehicle of each technology. Because of the multiple compilation and synthesis steps undertaken, the expectation that there should be inherent uncertainties at every step of the compilation, the lack of usable uncertainty analyses in our data sources, and for the sake of simplicity we decided not to introduce uncertainty at the prior calculation steps but rather to introduce uncertainty in the resulting MI coefficients (compare to the drive and battery technology shares coefficients described in section 4.2.2, in which uncertainties were introduced in the underlying calculation steps). Our decision is corroborated by the fact most materials of interest are dominant in one specific component (e.g. Nd in permanent magnets of electric motors), so the MI coefficient's uncertainty distribution should be virtually equal to that of the component. The uncertainties of the MI coefficients were drawn from normal distributions:

$$MI_{i,j,MC} \sim \mathcal{N}(MI_{i,j}, (0.1MI_{i,j})^2)$$

No uncertainties were introduced to the alternative MI figures of the two scenarios in which the AlCeMg alloy is introduced.

6.3 Uncertainty results

The uncertainties of the results obtained with the Monte Carlo simulations are complex functions of the underlying uncertainties introduced in the exogenous variables. Uncertainty in the exogenous variable results was found to vary over time, but some commonalities were found. In general, the distribution of the uncertainty in the endogenous variables is wider than in the exogenous variables. As detailed in SI section 4.2, the standard deviations of the normal distributions used to model uncertainty in the exogenous variables were set to be $\frac{1}{10}\mu$, i.e. 10% of their means μ . In comparison, the materials inflow and stocks results (endogenous variables) have standard deviations of $\frac{1}{6}\mu$ on average, and outflows uncertainty bands are even wider, $\frac{1}{4}\mu$ on average. The uncertainty ranges for all results are asymmetrically distributed with a positive skew and their median values are smaller than their means, supporting the observation that the uncertainties of the endogenous variables do not follow normal distributions.

Figures S7 and S8 present a full range of confidence bands (1%, 5%, 10%, 25%, 50%, 75%, 90%, 95% and 99%) obtained with the Monte Carlo simulations, using neodymium (Figure S6) as an example of a continuously growing stock and cerium (Figure S7) as an example of a material with a peak and decline. Below and in the main text and we discuss the 5% and 95% bands. The values of the confidence bands for vehicle results vary over time but are on average in the range of [-23%, 26%] for inflows and stocks and [-30%, 45%] for outflows (the expected range of corresponding normal distributions would be [$\pm 25\%$] and [$\pm 40\%$] respectively). 5% and 95% confidence bands for the inflow and outflow results of the

eight vehicle technologies are presented in Figure 1 of the main text. The next section describes the sensitivity of these results to the uncertainty in the endogenous variables.

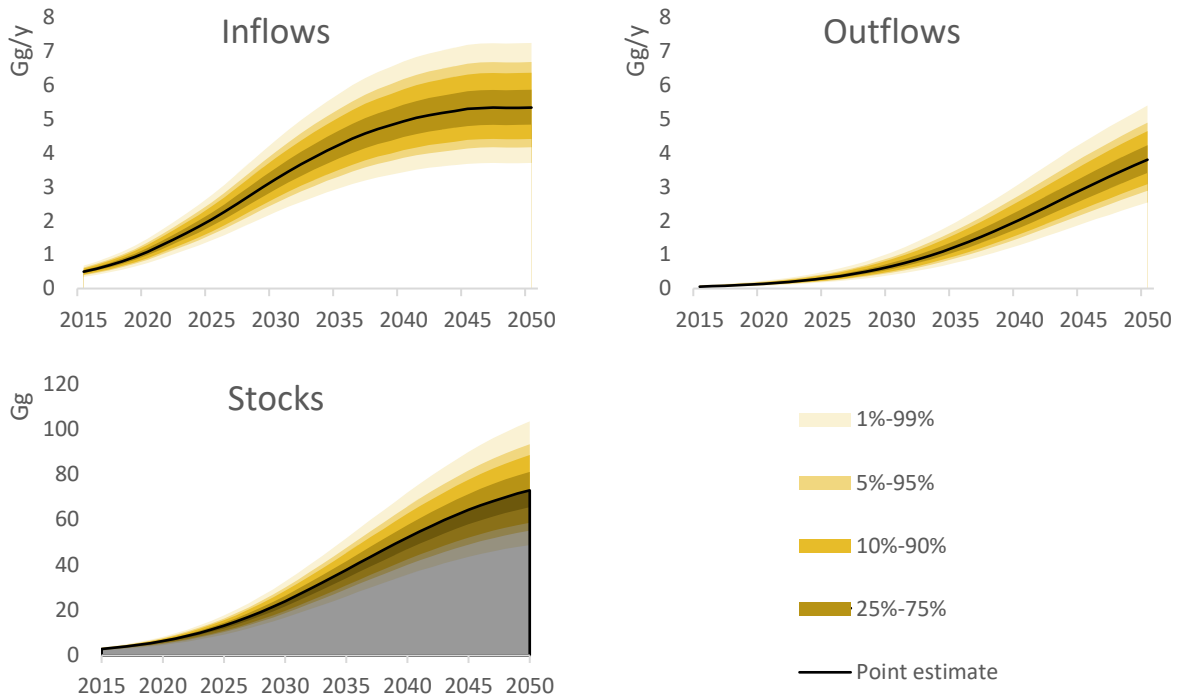


FIGURE S7: UNCERTAINTY IN THE RESULTS OF NEODYMIUM OBTAINED THROUGH MONTE CARLO SIMULATIONS.

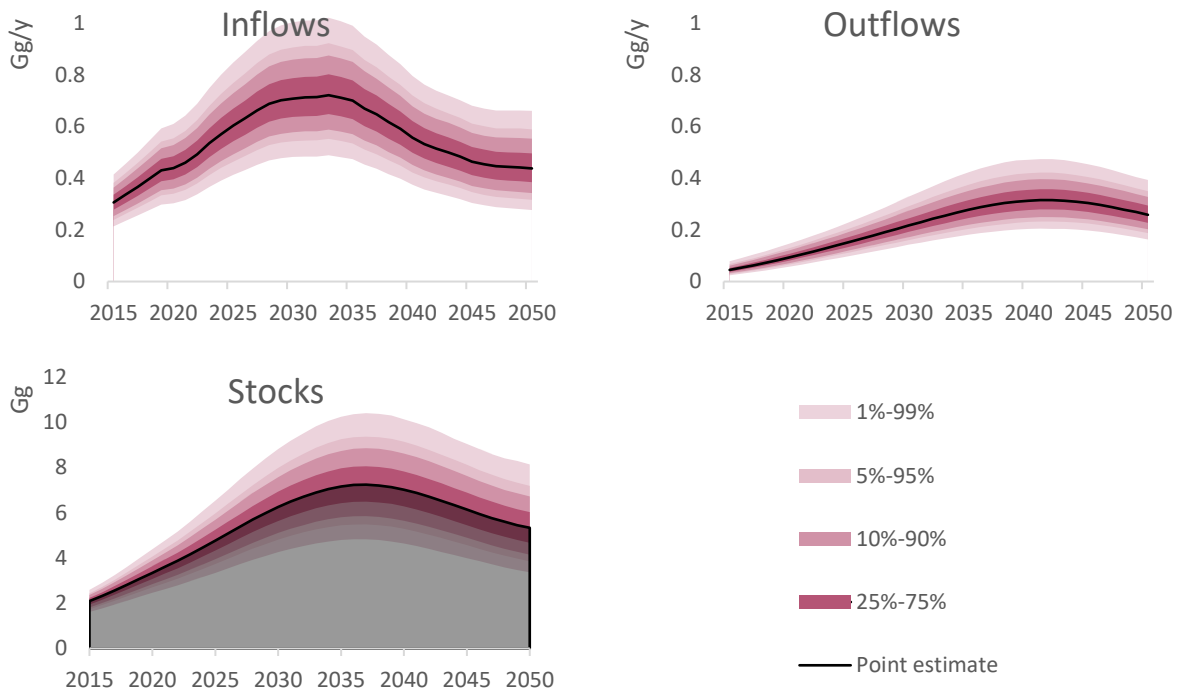


FIGURE S8: UNCERTAINTY IN THE RESULTS OF CERIUM OBTAINED THROUGH MONTE CARLO SIMULATIONS.

7 Global sensitivity analysis and attribution of uncertainty

7.1 Methods

The 12 exogenous variables for which stochasticity was introduced using Monte-Carlo simulations are expected to yield different influence on the results, depending on the relations between specific exogenous variables and endogenous variables (for example, lanthanum is only found in NiMH batteries, and the values and uncertainty of its results should therefore be independent of BEV related variables). We conducted a global sensitivity analysis using the method of normalized squares of Spearman's rank-correlation coefficients [40,41] to attribute the relative influence of each exogenous variable on the material mass results, and to also check whether these influences change over the time.

For each endogenous variable, twelve Spearman's rank-correlation coefficient ρ values were calculated using the sets of 10,000 results obtained with the Monte Carlo simulations, and for each time-step of the future portion of the model (2015-2050).

$$\rho_{EN,EX,t} = 1 - \frac{6 \sum_{MC=1}^n (\text{rank } EN_{MC,t} - \text{rank } EX_{MC,t})^2}{n(n^2 - 1)}$$

Where $\text{rank } EN_{MC,t}$ and $\text{rank } EX_{MC,t}$ are the ordinal rankings of the n Monte Carlo results of the endogenous variable EN and exogenous variable EX , respectively, at model time step t , and $n = 10,000$ Monte Carlo model runs.

The resulting 12 ρ values for each endogenous variable were then normalized in the following fashion:

$$C_{EN,EX,t} = \frac{(\rho_{EN,EX,t})^2}{\sum_{EX=1}^{12} (\rho_{EN,EX,t})^2}$$

Where $C_{EN,EX,t}$ is the normalized square of Spearman's rank-correlation coefficients, which allow comparisons and attribution of uncertainty in the exogenous variables to the uncertainty of the endogenous variable. The sum of $C_{EN,EX,t}$ for any given endogenous variable EN at model time step t is equal to 1.

7.2 Sensitivity analysis results

7.2.1 Common findings

Using the normalized squares of Spearman's rank-correlation coefficients, we find that most of the variance in the results can be attributed to only a handful of variables. In general, material inflow results are most sensitive to two variables: $\text{inflow}(t)$ (through s , the inflow variable's scaling factor described in SI section 4.2.1) and $MI_{i,j}$. Uncertainty in these two variables contribute almost equal shares to the variance in the inflow results of all materials at any point in time. The sensitivity of the results to the values of drive $d_{k,t}$ and battery technology $b_{k,l,t}$ shares that make up $v_{i,t}$ are small, although their

specific influences tend to change over time and vary between materials depending on the specific technologies they are associated with (see details for each material below).

Uncertainty in the stock results of all materials can be attributed mostly to $MI_{i,j}$ in 2015, but by 2025 the contribution of $inflow(t)$ grows to 30%-40% depending on the material. Variation in the Weibull survival curve's scale parameter a_2 grows in influence as time progresses, and contributes up to 10% of the uncertainty of the stocks results in 2050.

The outflow results are most sensitive to the characteristics of the survival curve, defined using shape parameter a_1 and scale parameter a_2 . The outflow results are more sensitive to changes in the value of the scale parameter than the shape parameter (cf. figure S4). The influence of the curve on the outflow results is stronger in the earlier modeling period and diminishes over time, as the stock gets "built up" with more cohorts. As time progresses, the outflow results become more sensitive to uncertainty in $inflow(t)$ and $MI_{i,j}$.

Figures S9-S14 present the contribution of uncertainty in each of the 12 exogenous variables to the variance in the results, and how these change over time.

The results of several exemplary materials are presented: the rare earth elements neodymium, cerium (lanthanum, terbium, erbium, and gadolinium's results are virtually identical), and dysprosium, as well as cobalt, lithium, and platinum to showcase how the sensitivity results of materials related to other technologies (li-ion and li-polymer batteries for cobalt and lithium, and fuel cells for platinum) compare to the rare earth elements.

For each material, figures for the inflow, stock, and outflow results 2015-2050 are presented. The horizontal axis is time t , and vertical axis is the values of $C_{EN,EX}$ in time t . The 12 EX variables are color coded in the following figures:

EX	Description	Uncertainty details
MI	Material intensity	SI section 4.2.4
$b_{HEV,NiMH}$	Share of NiMH batteries in the inflow of HEV vehicles	SI section 4.2.2.3
$b_{HEV,Li-ion}$	Share of Li-ion batteries in the inflow of HEV vehicles	SI section 4.2.2.3
$b_{FCV,NiMH}$	Share of NiMH batteries in the inflow of FCV vehicles	SI section 4.2.2.2
$b_{FCV,Li-ion}$	Share of Li-ion batteries in the inflow of FCV vehicles	SI section 4.2.2.2
d_{FCV}	Share of FCV in vehicle inflows	SI section 4.2.2.1
d_{BEV}	Share of BEV in vehicle inflows	SI section 4.2.2.1
d_{PHEV}	Share of PHEV in vehicle inflows	SI section 4.2.2.1
d_{HEV}	Share of HEV in vehicle inflows	SI section 4.2.2.1
a_2	Weibull survival curve scale parameter	SI section 4.2.3
a_1	Weibull survival curve shape parameter	SI section 4.2.3
$Inflow$	Scaling of the inflow curve	SI section 4.2.1

7.2.2 Neodymium

The results of neodymium have only a minute (~1%) sensitivity to variance in the relative shares of the various drive technologies and are not influenced by the shares of battery technologies, because neodymium's primary usage is in permanent magnets in electric motors.

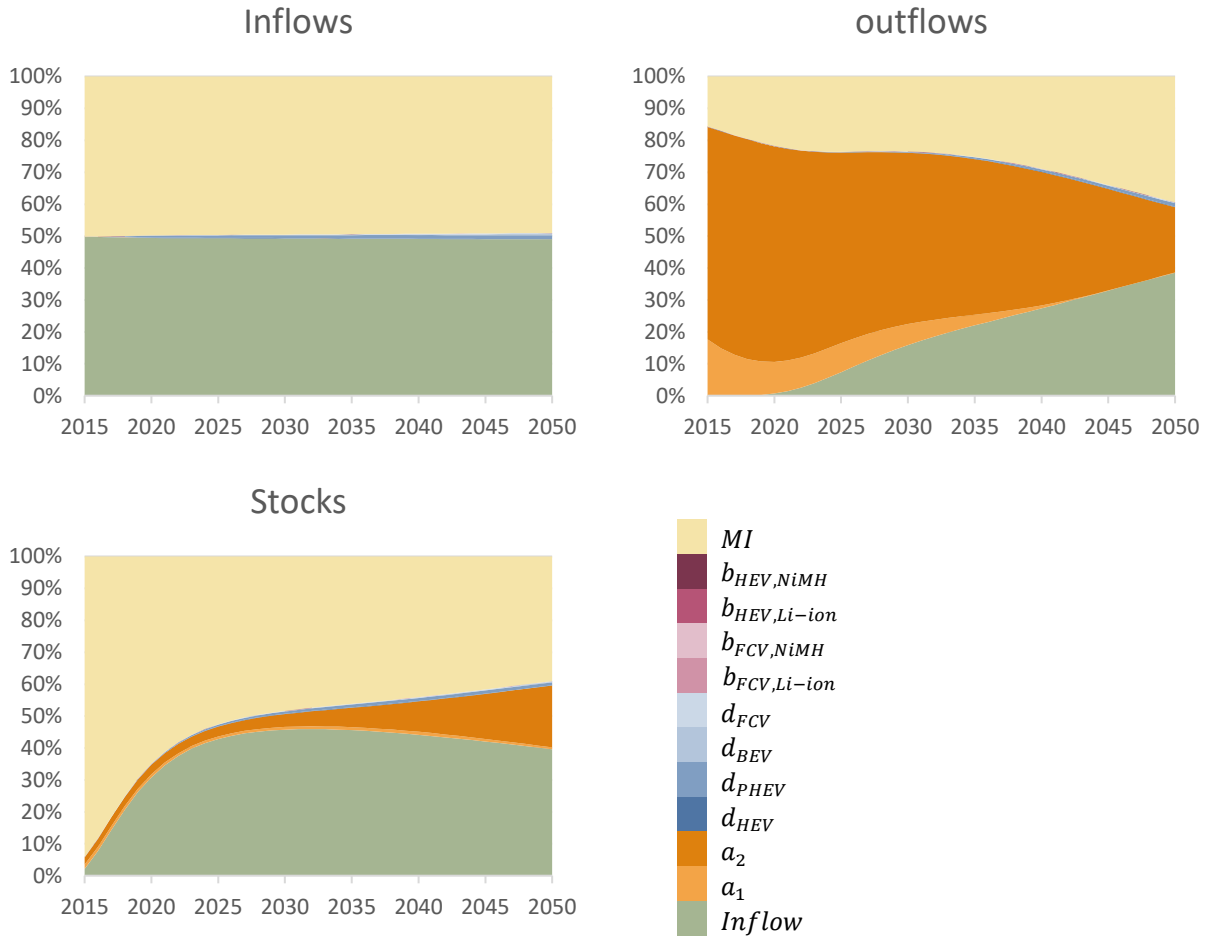


FIGURE S9: THE SHARE OF UNCERTAINTY IN THE INFLOWS, OUTFLOWS, AND STOCKS RESULTS OF NEODYMIUM ATTRIBUTED TO EACH RANDOMIZED EXOGENOUS VARIABLE IN EACH TIMESTEP. CALCULATED USING NORMALIZED SQUARE OF SPEARMAN'S RANK-CORRELATION COEFFICIENTS (SEE SI SECTION 5.1) OF THE MONTE CARLO SIMULATION RESULTS (SEE SI SECTION 4).

7.2.3 Cerium

Cerium's main usage (in the baseline scenario) is in NiMH batteries. Its results' sensitivity to uncertainties in the shares of the battery technologies $b_{HEV,NiMH}$ and $b_{FCV,NiMH}$ is high, as well as to the mix of drive technologies which utilize these battery types (HEV and FCV). The phasing out of HEV-NiMH and late growth of the FCV technologies can be seen in the changes of the influencing factors over time. The sensitivity analysis of the other rare earths found as mischmetal in NiMH (La, Pr, Gd, Er, and Tb) is the same as Ce.

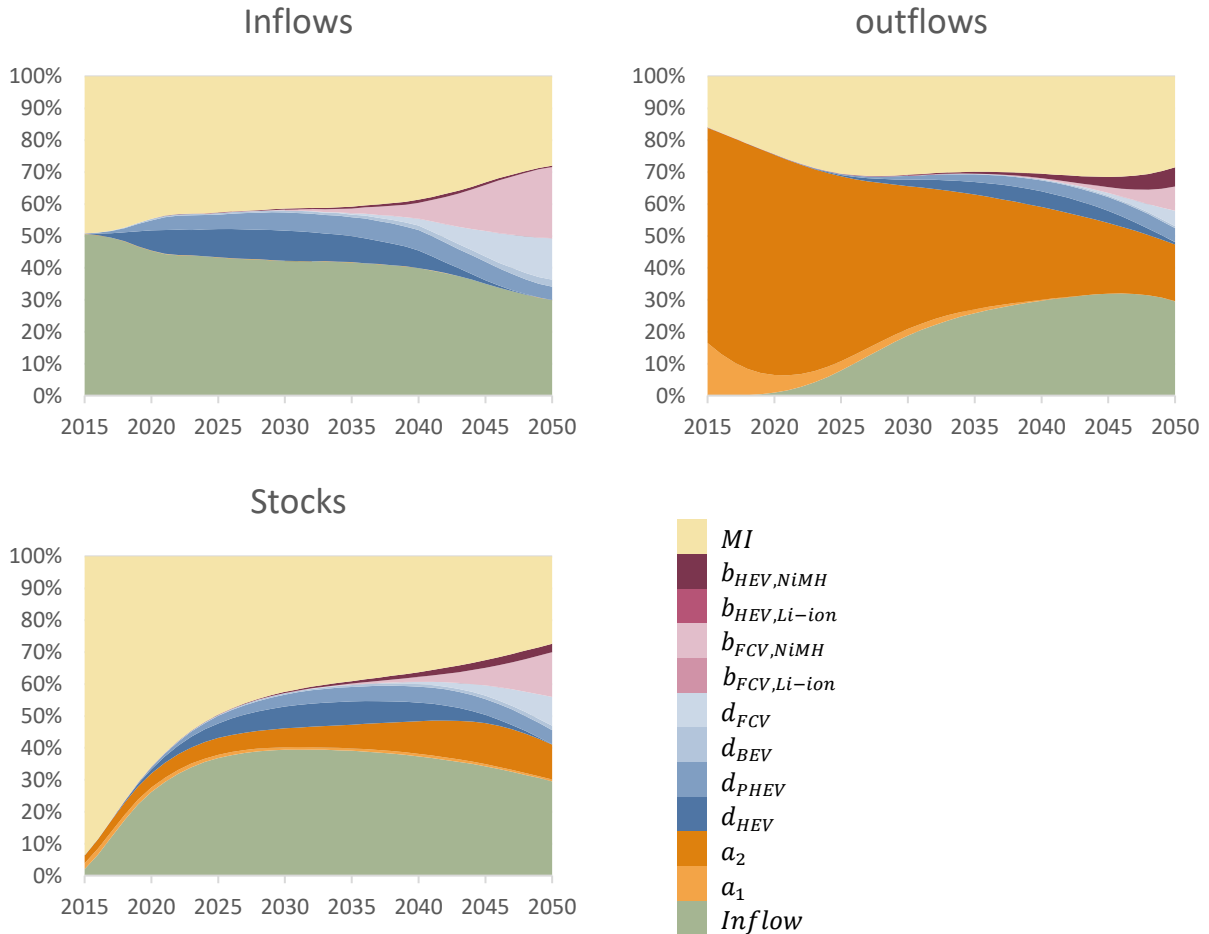


FIGURE S10: THE SHARE OF UNCERTAINTY IN THE INFLOWS, OUTFLOWS, AND STOCKS RESULTS OF CERIUM ATTRIBUTED TO EACH RANDOMIZED EXOGENOUS VARIABLE IN EACH TIMESTEP. CALCULATED USING NORMALIZED SQUARE OF SPEARMAN'S RANK-CORRELATION COEFFICIENTS (SEE SI SECTION 5.1) OF THE MONTE CARLO SIMULATION RESULTS (SEE SI SECTION 4).

7.2.4 Dysprosium

Dysprosium is used in all drive technologies, in permanent magnets in electric motors (as a companion to neodymium). However, it is also found in small amounts in mischmetal in NiMH batteries. For this reason, its results are somewhat more sensitive to uncertainty in the shares of vehicle technologies compared to neodymium.

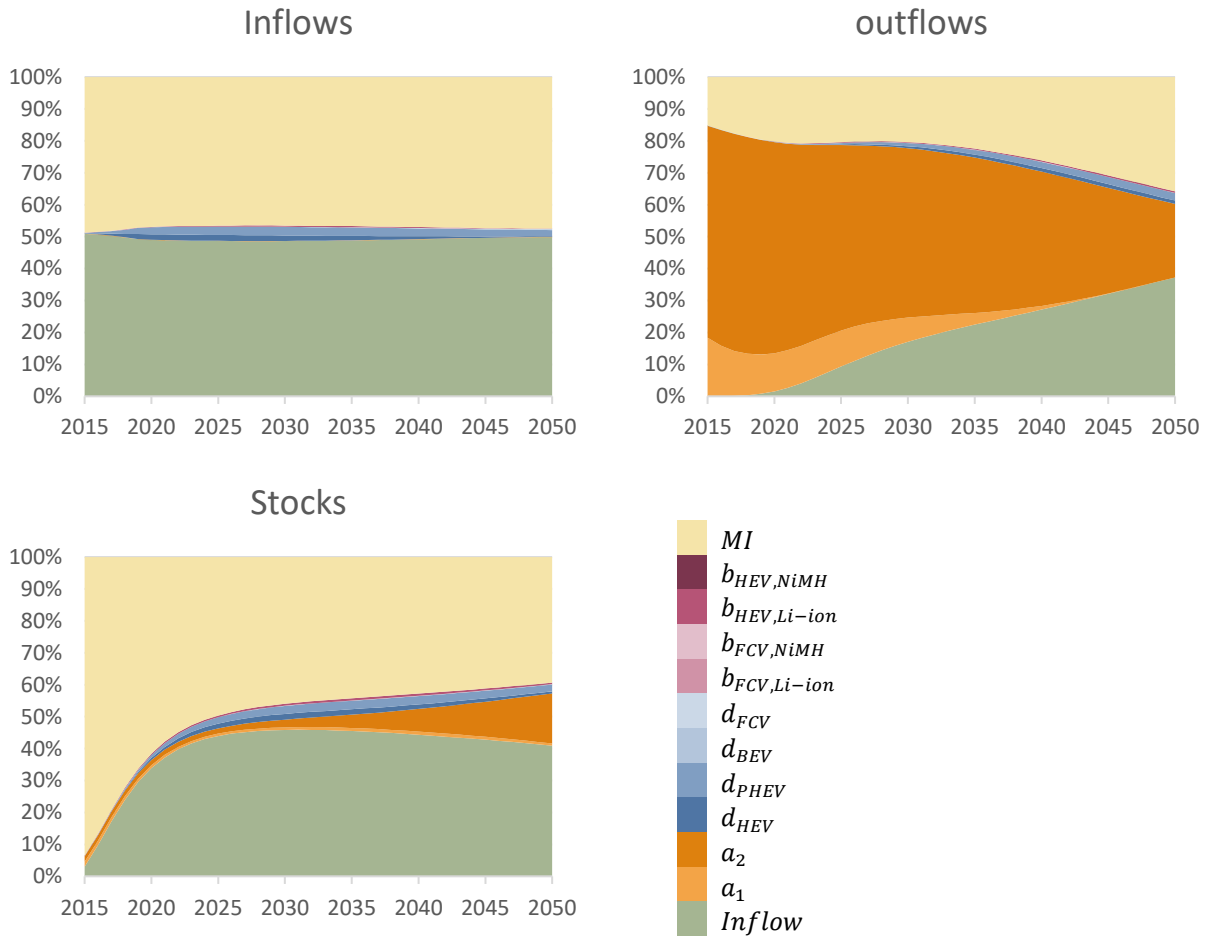


FIGURE S11: THE SHARE OF UNCERTAINTY IN THE INFLOWS, OUTFLOWS, AND STOCKS RESULTS OF DYSPROSIUM ATTRIBUTED TO EACH RANDOMIZED EXOGENOUS VARIABLE IN EACH TIMESTEP. CALCULATED USING NORMALIZED SQUARE OF SPEARMAN'S RANK-CORRELATION COEFFICIENTS (SEE SI SECTION 5.1) OF THE MONTE CARLO SIMULATION RESULTS (SEE SI SECTION 4).

7.2.5 Cobalt

The results for cobalt are sensitive to the shares of HEV and BEV in the inflows. As HEV vehicle inflows are overtaken by other technologies, its influence on cobalt inflows and stocks results diminishes. Interestingly, the shares of the different battery technology types have no influence on the results, perhaps because the two major drive technologies by vehicle numbers, PHEV and BEV, use solely the Li-ion battery technology.

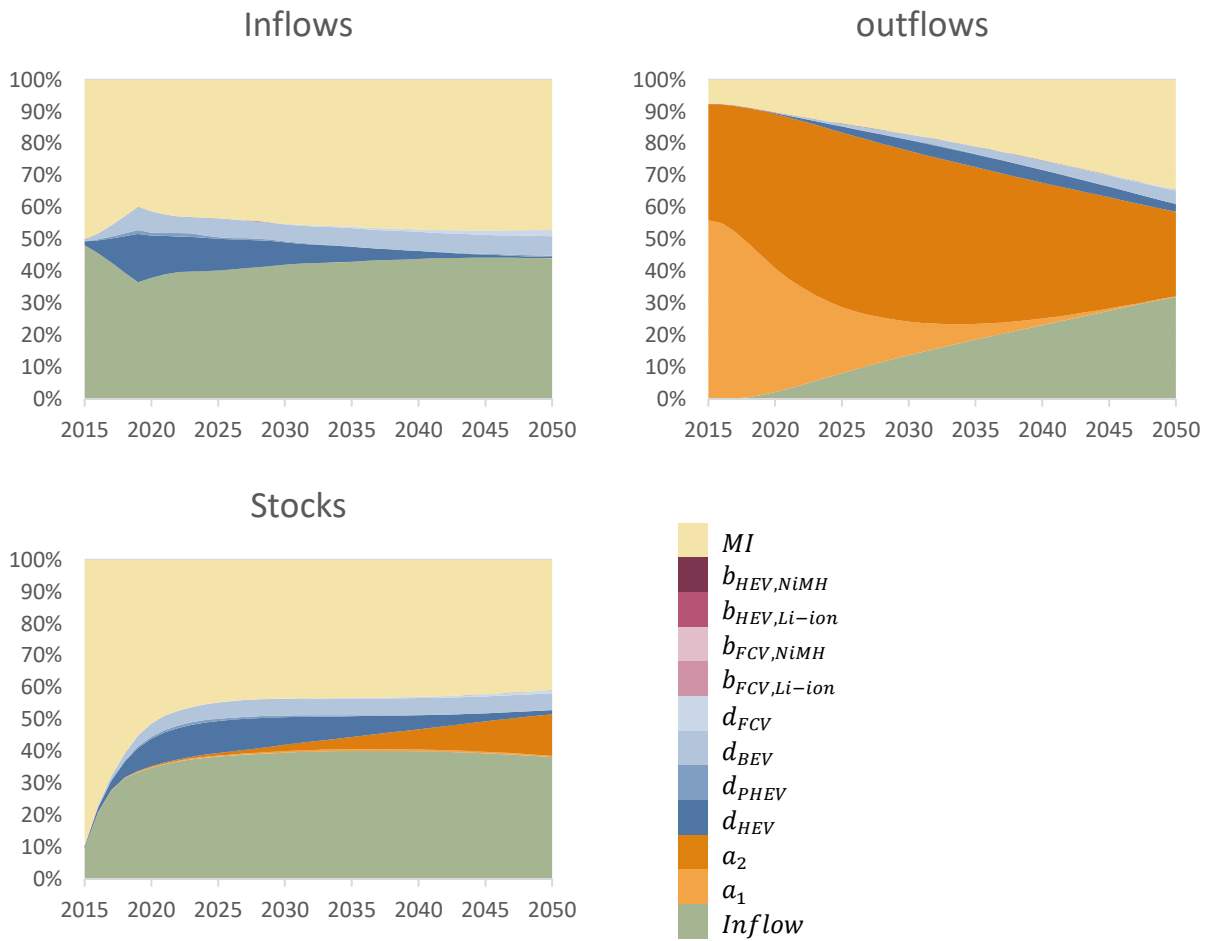


FIGURE S12: THE SHARE OF UNCERTAINTY IN THE INFLOWS, OUTFLOWS, AND STOCKS RESULTS OF COBALT ATTRIBUTED TO EACH RANDOMIZED EXOGENOUS VARIABLE IN EACH TIMESTEP. CALCULATED USING NORMALIZED SQUARE OF SPEARMAN'S RANK-CORRELATION COEFFICIENTS (SEE SI SECTION 5.1) OF THE MONTE CARLO SIMULATION RESULTS (SEE SI SECTION 4).

7.2.6 Lithium

The sensitivity of lithium results to uncertainties in the exogenous variables is remarkably similar to cobalt, underscoring the companionship of these two materials in their end-uses in AEVs, in Li-ion and Li-polymer batteries.

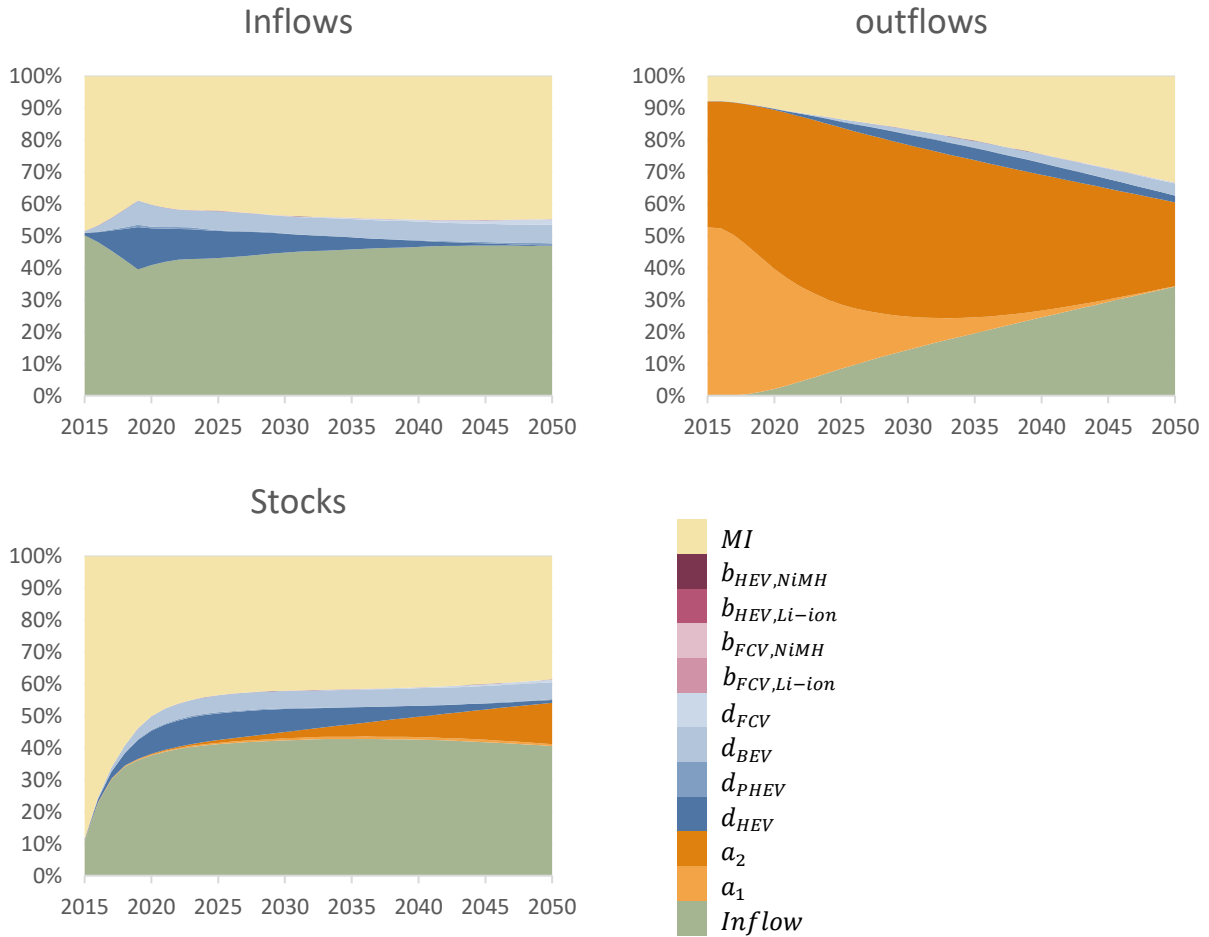


FIGURE S13: THE SHARE OF UNCERTAINTY IN THE INFLOWS, OUTFLOWS, AND STOCKS RESULTS OF LITHIUM ATTRIBUTED TO EACH RANDOMIZED EXOGENOUS VARIABLE IN EACH TIMESTEP. CALCULATED USING NORMALIZED SQUARE OF SPEARMAN'S RANK-CORRELATION COEFFICIENTS (SEE SI SECTION 5.1) OF THE MONTE CARLO SIMULATION RESULTS (SEE SI SECTION 4).

7.2.7 Platinum

Although platinum is found in catalytic converters in HEVs and PHEVs, it is used in higher intensities in FCVs. The sensitivity of the platinum results to the share of FCVs in the inflows grows over time.

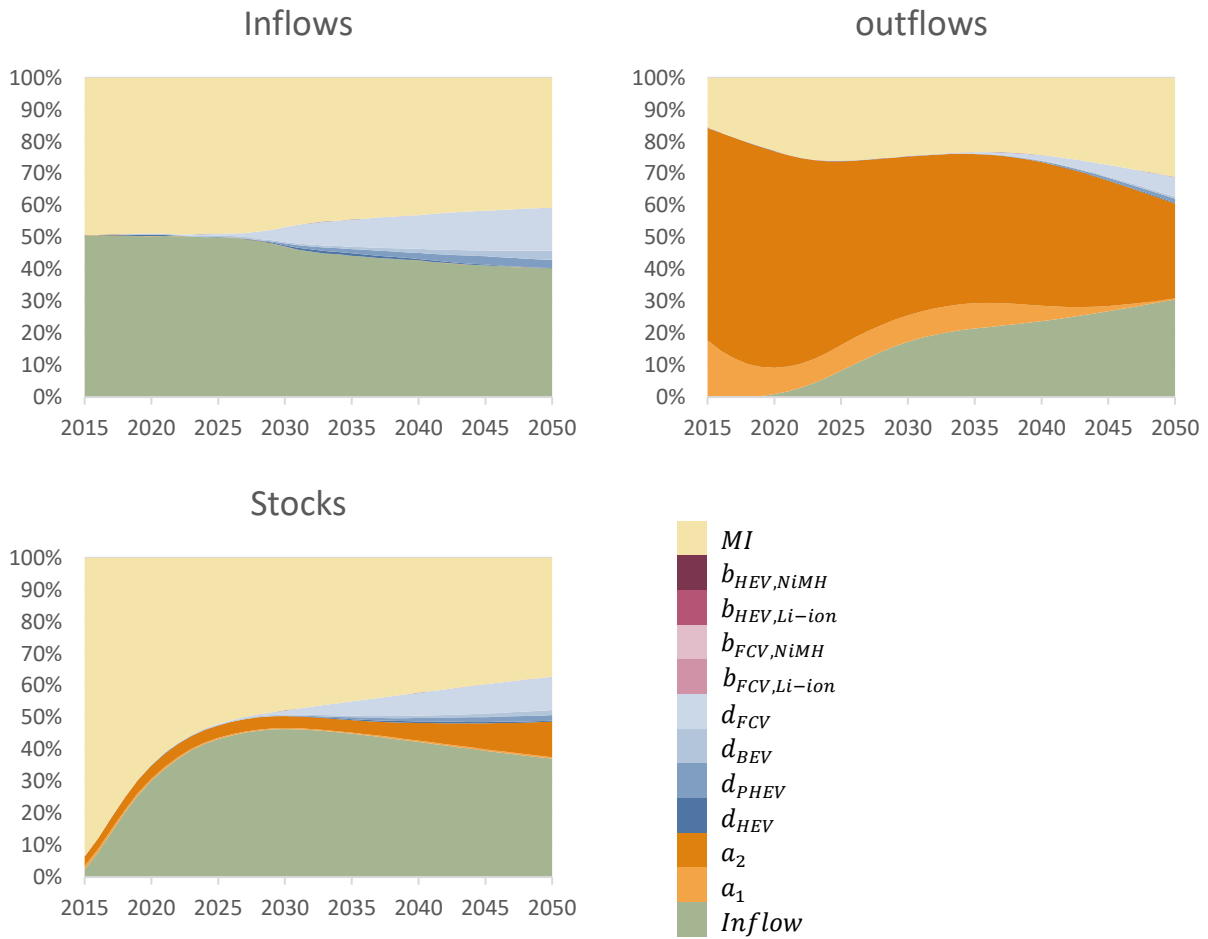


FIGURE S14: THE SHARE OF UNCERTAINTY IN THE INFLOWS, OUTFLOWS, AND STOCKS RESULTS OF PLATINUM ATTRIBUTED TO EACH RANDOMIZED EXOGENOUS VARIABLE IN EACH TIMESTEP. CALCULATED USING NORMALIZED SQUARE OF SPEARMAN'S RANK-CORRELATION COEFFICIENTS (SEE SI SECTION 5.1) OF THE MONTE CARLO SIMULATION RESULTS (SEE SI SECTION 4).

8 References

1. Brunner, P. H.; Rechberger, H. *Practical handbook of material flow analysis*; Lewis Publishers: Boca Raton, 2004; ISBN 1-56670-604-1.
2. Fishman, T.; Schandl, H.; Tanikawa, H.; Walker, P.; Krausmann, F. Accounting for the Material Stock of Nations. *Journal of Industrial Ecology* **2014**, *18*, 407–420, doi:10.1111/jiec.12114.
3. U.S. Department of Energy Alternative Fuels Data Center Available online: <https://www.afdc.energy.gov/data/>.
4. Chan, C. C.; Bouscayrol, A.; Chen, K. Electric, hybrid, and fuel-cell vehicles: Architectures and modeling. *IEEE transactions on vehicular technology* **2010**, *59*, 589–598.
5. Toyota Motor Corporation *2017 Camry*; 2016;
6. Toyota Motor Corporation *2010 Prius Specifications*; 2010;
7. KIA Motors America, Inc. *2017 Optima Hybrid / Plug-in Hybrid*; 2016;
8. Nissan Motor Co., Ltd. *2017 Nissan Leaf*; 2016;
9. Toyota Motor Corporation *2017 Mirai Product Information*; 2016;
10. Toyota Motor Corporation *Toyota 2016 Mirai Owners Manual*; 2015;
11. U.S. Department of Energy AVTA: Light Duty Alternative Fuel and Advanced Vehicle Data Available online: <https://energy.gov/eere/vehicles/avta-light-duty-alternative-fuel-and-advanced-vehicle-data>.
12. Ellingsen, L. A.-W.; Majeau-Bettez, G.; Singh, B.; Srivastava, A. K.; Valøen, L. O.; Strømman, A. H. Life Cycle Assessment of a Lithium-Ion Battery Vehicle Pack. *Journal of Industrial Ecology* **2014**, *18*, 113–124, doi:10.1111/jiec.12072.
13. Majeau-Bettez, G.; Hawkins, T. R.; Strømman, A. H. Life Cycle Environmental Assessment of Lithium-Ion and Nickel Metal Hydride Batteries for Plug-In Hybrid and Battery Electric Vehicles. *Environmental Science & Technology* **2011**, *45*, 4548–4554, doi:10.1021/es103607c.
14. Yano, J.; Muroi, T.; Sakai, S. Rare earth element recovery potentials from end-of-life hybrid electric vehicle components in 2010–2030. *Journal of Material Cycles and Waste Management* **2016**, *18*, 655–664, doi:10.1007/s10163-015-0360-4.
15. Hawkins, T. R.; Singh, B.; Majeau-Bettez, G.; Strømman, A. H. Comparative Environmental Life Cycle Assessment of Conventional and Electric Vehicles. *Journal of Industrial Ecology* **2013**, *17*, 53–64, doi:10.1111/j.1530-9290.2012.00532.x.
16. Hawkins, T. R.; Singh, B.; Majeau-Bettez, G.; Strømman, A. H. Corrigendum to: Hawkins, T. R., B. Singh, G. Majeau-Bettez, and A. H. Strømman. 2012. Comparative environmental life cycle assessment of conventional and electric vehicles. *Journal of Industrial Ecology* DOI: 10.1111/j.1530-9290.2012.00532.x. *Journal of Industrial Ecology* **2013**, *17*, 158–160, doi:10.1111/jiec.12011.
17. Elshkaki, A. An analysis of future platinum resources, emissions and waste streams using a system dynamic model of its intentional and non-intentional flows and stocks. *Resources Policy* **2013**, *38*, 241–251, doi:http://dx.doi.org/10.1016/j.resourpol.2013.04.002.
18. Sun, Y.; Delucchi, M.; Ogden, J. The impact of widespread deployment of fuel cell vehicles on platinum demand and price. *International Journal of Hydrogen Energy* **2011**, *36*, 11116–11127, doi:http://dx.doi.org/10.1016/j.ijhydene.2011.05.157.
19. Tollefson, J. Worth its weight in platinum: booming mineral prices leave car makers scrambling to eke more catalytic performance out of precious metals. *Nature* **2007**, *450*, 334–336, doi:doi:10.1038/450334a.

20. Borgwardt, R. H. Platinum, fuel cells, and future US road transport. *Transportation Research Part D: Transport and Environment* **2001**, *6*, 199–207, doi:[http://dx.doi.org/10.1016/S1361-9209\(00\)00023-7](http://dx.doi.org/10.1016/S1361-9209(00)00023-7).
21. TIAX LLC *Platinum Availability and Economics for PEMFC Commercialization. Report to US Department of Energy*; 2003;
22. Cullbrand, K.; Magnusson, O. *The use of potentially critical materials in passenger cars*; Chalmers University of Technology: Gothenburg, Sweden, 2012;
23. Restrepo, E.; Løvik, A. N.; Wäger, P.; Widmer, R.; Lonka, R.; Müller, D. B. Stocks, Flows, and Distribution of Critical Metals in Embedded Electronics in Passenger Vehicles. *Environmental Science & Technology* **2017**, *51*, 1129–1139, doi:10.1021/acs.est.6b05743.
24. Alonso, E.; Wallington, T.; Sherman, A.; Everson, M.; Field, F.; Roth, R.; Kirchain, R. An assessment of the rare earth element content of conventional and electric vehicles. *SAE International Journal of Materials and Manufacturing* **2012**, *5*, 473–477.
25. Alonso, E.; Sherman, A. M.; Wallington, T. J.; Everson, M. P.; Field, F. R.; Roth, R.; Kirchain, R. E. Evaluating Rare Earth Element Availability: A Case with Revolutionary Demand from Clean Technologies. *Environmental Science & Technology* **2012**, *46*, 3406–3414, doi:10.1021/es203518d.
26. Cheah, L.; Heywood, J.; Kirchain, R. The energy impact of US passenger vehicle fuel economy standards. In *IEEE International Symposium on Sustainable Systems and Technology (ISSST)*; IEEE, 2010; pp. 1–6.
27. Du, X.; Restrepo, E.; Widmer, R.; Wäger, P. Quantifying the distribution of critical metals in conventional passenger vehicles using input-driven and output-driven approaches: a comparative study. *Journal of Material Cycles and Waste Management* **2015**, *17*, 218–228, doi:10.1007/s10163-015-0353-3.
28. U.S. Department of Transportation *National Transportation Statistics*; Bureau of Transportation Statistics, Washington DC, 2016;
29. Hyndman, R. J.; Athanasopoulos, G. *Forecasting: principles and practice*; OTexts, 2014; ISBN 978-0-9875071-0-5.
30. StataCorp nl — Nonlinear least-squares estimation. In *Stata Base Reference Manual*; Stata Press: College Station, Texas, 2015; pp. 1673–1693 ISBN 978-1-59718-164-8.
31. U.S. Geological Survey *Mineral Commodity Summaries 2017*; 2017th ed.; Reston, VA, 2017;
32. Liu, G.; Müller, D. B. Centennial Evolution of Aluminum In-Use Stocks on Our Aluminized Planet. *Environmental Science & Technology* **2013**, *47*, 4882–4888, doi:10.1021/es305108p.
33. Laner, D.; Rechberger, H.; Astrup, T. Systematic Evaluation of Uncertainty in Material Flow Analysis. *Journal of Industrial Ecology* **2014**, *18*, 859–870, doi:10.1111/jiec.12143.
34. Krausmann, F.; Wiedenhofer, D.; Lauk, C.; Haas, W.; Tanikawa, H.; Fishman, T.; Miatto, A.; Schandl, H.; Haberl, H. Global socioeconomic material stocks rise 23-fold over the 20th century and require half of annual resource use. *Proceedings of the National Academy of Sciences* **2017**, *114*, 1880–1885, doi:10.1073/pnas.1613773114.
35. Morgan, M. G.; Henrion, M. *Uncertainty: a guide to dealing with uncertainty in quantitative risk and policy analysis*; 8th Edition.; Cambridge university press: Cambridge UK, 2006;
36. Plugincars.com The Risks of Using Hybrid Sales to Forecast Growth of Electric Cars Available online: <http://www.plugincars.com/risks-using-hybrid-sales-forecast-growth-electric-cars-128566.html>.
37. Miatto, A.; Schandl, H.; Tanikawa, H. How important are realistic building lifespan assumptions for material stock and demolition waste accounts? *Resources, Conservation and Recycling* **2017**, *122*, 143–154, doi:<http://dx.doi.org/10.1016/j.resconrec.2017.01.015>.
38. Kapur, A.; Keoleian, G.; Kendall, A.; Kesler, S. E. Dynamic Modeling of In-Use Cement Stocks in the United States. *Journal of Industrial Ecology* **2008**, *12*, 539–556, doi:10.1111/j.1530-9290.2008.00055.x.

39. National Highway Traffic Safety Administration *Vehicle Survivability and Travel Milage Schedules*; NHTSA Technical Report; U.S. Department of Transportation: Springfield, VA, 2006;
40. Gautheir, T. D. Detecting Trends Using Spearman's Rank Correlation Coefficient. *Environmental Forensics* **2001**, 2, 359–362, doi:10.1080/713848278.
41. Cao, Z.; Shen, L.; Zhong, S.; Liu, L.; Kong, H.; Sun, Y. A Probabilistic Dynamic Material Flow Analysis Model for Chinese Urban Housing Stock. *Journal of Industrial Ecology* **2017**, n/a–n/a, doi:10.1111/jiec.12579.